JOURNAL OF MATERIALS SCIENCE 31 (1996) 323–334

Microwave absorbent: preparation, mechanical properties and r.f.–microwave conductivity of SiC (and/or mullite) fibre reinforced Nasicon matrix composites

E. MOUCHON, PH. COLOMBAN*
ONERA, OM, BP 72, 92322 Chatillon, France

The electrical and mechanical properties of composites made with Nicalon® NLM202 SiC (and Nextel® 440) woven fibres in a sol–gel prepared Nasicon matrix are reported. Local microhardness, interfacial shear stress and three point flexural strength have been determined and correlated to the conclusion of an X-ray microanalysis of the fibre–matrix interphases. The radio frequency (r.f.) to microwave conductivity of the composites has been measured and compared with that of their constituents (Nasicon matrix, SiC fibre) and with the direct current (d.c.) conductivity of extracted fibres.

1. Introduction

Stealthiness is now a required specification for modern weapons, and parts made of specific materials may be used to absorb the emitted electromagnetic energy and to minimize the wave reflected in the direction of the enemy radar receiver. In some applications, e.g. high velocity missiles, the materials may undergo high thermomechanical stress. For these applications the most promising class of new materials is ceramic woven fabric reinforced ceramic matrix composites. The great weakness of monolithic ceramics is their intrinsic inability to tolerate mechanical damage without brittle rupture because of their polycrystalline nature and the type of chemical bonds existing in these compounds. The use of long, continuous ceramic fibres embedded in a refractory ceramic matrix results in a composite material exhibiting greater toughness through a specific micromechanism at the fibre–matrix interface: the cracks appearing in the matrix are deflected, dissociated and then stopped at the fibre–matrix interface [1], and the composite materials exhibit a fibrous, pseudoplastic fracture. Thus, knowledge of the ultimate strength allows the choice of acceptable load, and calculations with safety coefficients would thus be made for the part design.

The conducting properties of a composite should depend on the fibres, the matrix, the interface (or interphases) and on other parameters, such as the microstructure, the topology etc. At present, Nicalon® SiC fibres and Nextel® mullite fibres are considered the most convenient commercial fibres for the preparation of oxide matrix composites. Nicalon fibres exhibit semiconducting properties [2], whereas mullite fibres are pure dielectric [3]. To date composites have been only designed for their thermomechanical properties (see [4, 5]). In this paper, the preparation and mechanical and electrical properties (from d.c. to microwave frequency) of Nasicon matrix composites reinforced with long semiconducting and/or dielectric fibres are reported and discussed. The Nasicon solid solution, with the structural formula $Na_{1+x}Zr_2Si_xP_{3-x}O_{12}$ ($0 \leq x \leq 3$), has been extensively investigated for the last twenty years, due to its potential applications in superionic batteries and sensors [6]. For microwave absorbant preparation, Nasicon offers the advantage of an electrical conductivity varying by four orders of magnitude as a function of x. Furthermore, this material exhibits the rather low thermal expansion [7, 8] required for a composite matrix reinforced with SiC fibres. SiC and mullite fibre-reinforced Nasicon matrix composites appear, thus, to be a good system for the study of problems associated with the preparation of ceramic matrix composites (CMCs) with tailored microwave properties.

2. Experimental procedure

2.1. Composite preparation: the sol–gel process

The preparation process for two-dimensional woven fabric reinforced composites is based on the hydrolysis–polycondensation of alkoxides according to the following reaction [9–10].

$$MOR_n + H_2O \rightarrow M(OR)_{n-1}(OH) + R\vec{O}H$$

The resulting compound is a gel (composition: $MO_{n-x}(OH)_{2x}mH_2O$) which is converted by thermal treatment above 300 °C into a meso/microporous xerogel or "glass". The departure of the last OH^-

*Also at CNRS, LASIR, 2 rue Henri Dunant, 94320 Thiais, France. Author to whom correspondence should be addressed.

0022–2461

species leads to a dense glass, a glass–ceramic or a ceramic, depending on composition [9–14].

CMC preparation takes place in three stages [15–17]

1. Impregnation of the fibre yarns of the fabric with an interface (interphase) precursor: a liquid alkoxide mixture which slowly hydrolyses and polycondenses into a gel, *in situ*, by reaction with air moisture.

2. Deposition of a fine amorphous and reactive matrix precursor: a gel powder which has been heated to 700 °C, in air, in order to evacuate most of the protons and hence to reduce the shrinkage. This powder precursor is deposited onto the polymerized interface precursor–impregnated fabric in the form of a suspension in chlorobenzene with the addition of poly(methylmetacrylate) (PMMA) (2–4% in weight).

3. Hot pressing of the impregnated and stacked fabrics in a graphite mould at a temperature between 1000 and 1100 °C. Details of the manufacturing technology are given in [15].

This preparation route allows one to manufacture composites combining various matrices (mullite, zirconia, celsian, aluminum titanate) and woven fibres (of SiC, mullite, alumina); different kinds of matrix and fabric can be combined in the same composite [15–20].

2.2. Woven fabrics

Nicalon® NLM202 fibres (Nippon Carbon Co.) were woven along four directions (four dir) in the plane to give a ~ 1 mm thick fabric (four dir fabric, surface mass 76×10^{-3} g cm^{-3}) and along two directions in the plane to give a ~ 0.4 mm thick satin (interlacing each eighth fibre). The SiC fibre diameter is ~ 15 μm. The yarn contains ~ 500 fibres. The interlaced yarn network is shown in Fig. 1.

Nextel 440® mullite fibres (3M Co.) were woven along two directions in the plane to give a ~ 0.4 mm thick eight-satin (surface mass 22×10^{-3} g cm^{-3}). The mullite fibre diameter is about 11 μm and the yarn contains 390 fibres. Photographs of the fabric are shown in [6].

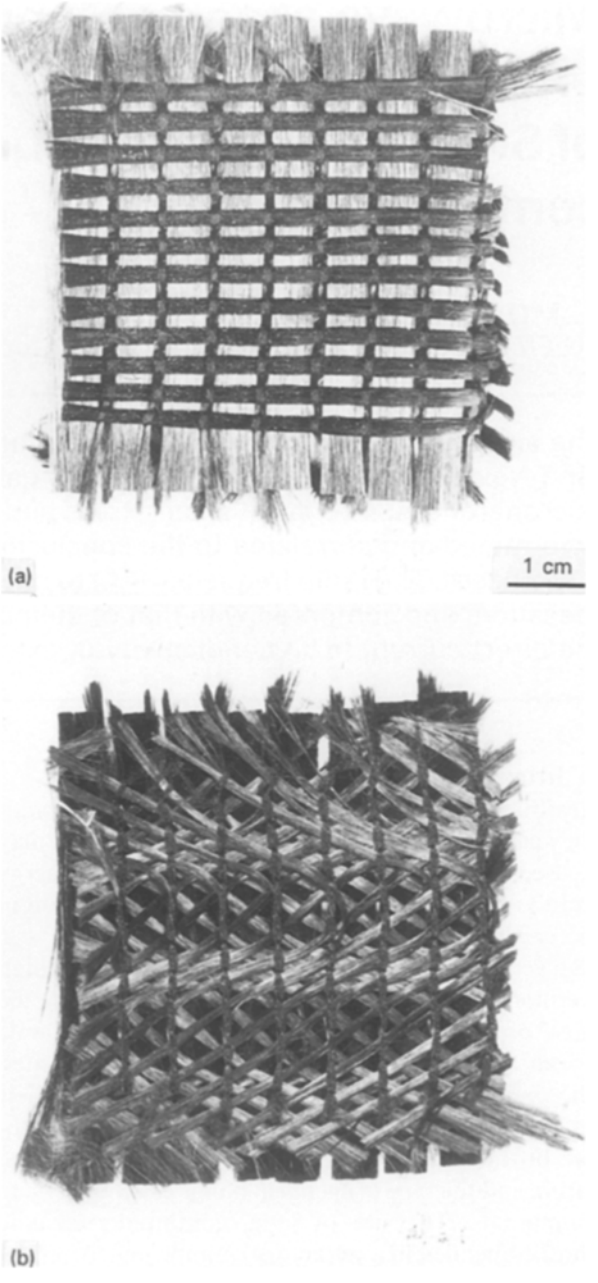

Figure 1 Photograph of a four dir woven fabric made of SiC Nicalon® NLM 202 fibres: (a) upper side, (b) under side.

2.3. Nasicon matrix precursor

Gel powder with $Na_{2.9}Zr_2Si_{1.9}P_{1.1}O_{12}$ composition ($x = 1.9$) was prepared using a sol–gel route previously described by Perthuis and Colomban [21]: a mixture of zirconium isopropoxide, silicon ethoxide and tributylphosphate was diluted in an equal volume of isopropanol and hydrolysed by an NaOH aqueous solution. The gel was dried under infrared (i.r.) bulbs. The resulting powder was heated to 700 °C for 2 h in air.

2.4. Interface/interphase precursor

The presence of a woven fabric makes the sintering between powder grains difficult: (a) the transmission of the applied pressure is inhibited and (b) the "inert", geometrically stable, nature of the fibre array means that shrinkage necessarily causes crack formation. Furthermore, depositing an item within the yarns in the fabric, through the voids between the fibres (a few micrometres, or less, in size) is very difficult. This is only possible using gaseous or liquid ceramic precursors, which are converted into ceramic with a yield which is necessarily low (≤ 0.5). It results in considerable shrinkage, which generates new voids: the presence of the woven fabric inhibits coherent shrinkage of the sample. In the case of two-dimensional reinforcements this dilemma is solved by the use of a very reactive matrix precursor in combination with an interface/interphase precursor. This

1. polycondenses within the fibre yarns into a gel,
2. is converted by heating into a glass–ceramic and simultaneously gives rise to a temporary liquid sintering aid in the same temperature range in which the matrix densification occurs, and

3. may (or not) react with the fibres to give a sliding interface.

The liquid phase contributes to the densification by mass transport (liquid assisted sintering), but also helps to lubricate the powder arrangement under pressure and to maximize the amount of contact between ceramic grains of pyrolysed matrix and interface precursors, despite the presence of the fibre network (fibre volume: 35–40%). Fig. 2 compares the shrinkage plot of the Nasicon matrix precursor and the interface precursor (a gel) with the evolution of the sample thickness during the hot pressing cycle. The Nasicon matrix precursor, previously heated to 700 °C, sinters at about 900 °C; at which temperature the mesoporosity disappears simultaneously with the nucleation of a rhombohedral, disordered Nasicon phase [22]. The monoclinic phase is obtained if the sintering temperature is between 1050 and 1250 °C [22, 23]. The sample shrinkage starts immediately upon heating via the dehydration of the interface precursor gel ($\leqslant 300$ °C) and continues at higher temperatures via the viscous creep of the gel under pressure. The main shrinkage takes place with matrix densification (> 800 °C) and with apparition of the liquid phase due to the boron oxide content. The effect of liquid

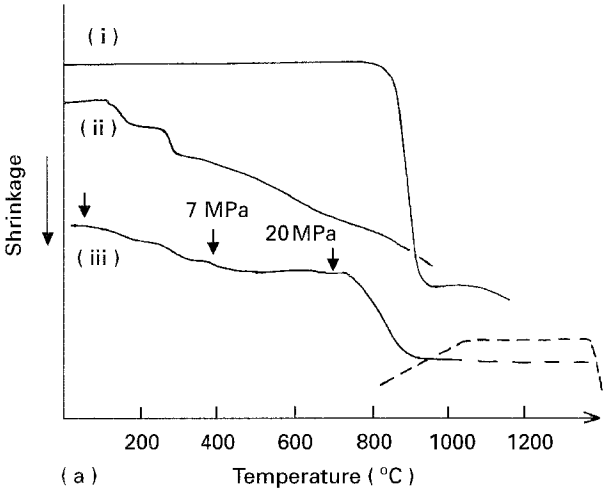

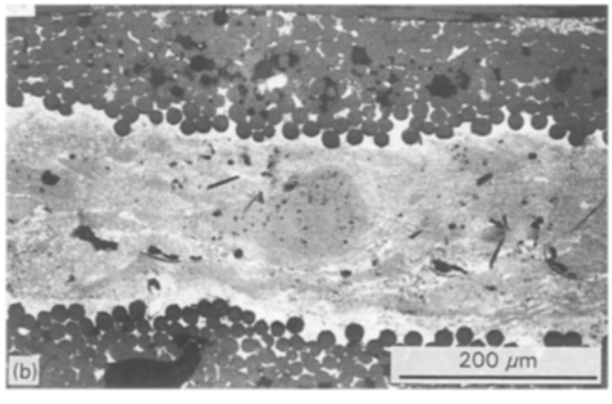

Figure 2 (a) Shrinkage plots of $x = 1.9$ Nasicon matrix previously heated at 700 °C (i) and of the Zr–Si–P–B interface precursor (ii) versus temperature and of the whole composite preform during the hot pressing cycle (iii) versus temperature up to 1035 °C.; The dashed line shows the temperature versus time run above 800 °C. Arrows indicate the steps of pressure increase. (b) SEM photomicrograph of a polished section of a composite prepared using TBB as interface precursor (SiC fibre satin fabric).

sintering is complete at about 1050 °C. Fig. 2 gives an illustration of the influence of the liquid phase. In order to observe the phenomenon more clearly, the interface precursor used in this case was pure tributylborate which gives rise to a large quantity of liquid phase, and a large thickness of Nasicon matrix was deposited on the fabric. Reaction between the boron oxide-rich liquid and the Nasicon precursor leads to zirconia precipitation, which appears as white on the photomicrographs giving an illustration of the liquid phase motion. The variety of fabric wearing plays a role on the sintering. Fabrics which have large interconnected voids between the yarns, e.g. the four dir fabric, may be preferred to fabrics having only small voids, e.g. the eight-satin, for the production of a composite with a continuous change of composition from the pure Nasicon matrix in between two sheet fabrics to the pure interface precursor in yarns at the centre of the fabric sheet.

The composition of the interface/interphase precursor must be chosen according to many requirements:

1. sintering temperature similar to that of the matrix,
2. generation of volatile liquid as a sintering aid,
3. formation of a "good" fibre–matrix interface, and
4. thermal expansion (the thermal expansion of the pyrolysed Zr–Si–P–B interface precursor is $3.2 \times 10^{-6}\,°C^{-1}$) intermediate between those of the fibre (SiC: $3.1 \times 10^{-6}\,°C^{-1}$) and the matrix ($5.5 \times 10^{-6}\,°C^{-1}$). The composition of the Zr–Si–P–B interface precursor is a mixture of tetraethoxyorthosilicate (TEOS, 1 volume), tributylborate(TBB, 1.8 volume), tributylphosphate (TBP, 1.8 volume) and zirconium isopropoxide (ZrP, 1 volume), and is very similar to that of Nasicon except for the absence of sodium. The corresponding resulting oxide composition is $ZrO_2 2SiO_2 1.5P_2O_5 1.5Br_2O_3$. The addition of boron compensates for the lack of sodium, maintaining a low sintering temperature (and enables the generation of a liquid phase above 600 °C). The use of a sodium-free interphase reduces the reaction between the fibre and sodium ions. Fig. 3 gives an example of a line scan performed for Na and Si across the composite interfabric region: one observes the confinement of Na in the interslab matrix and in the voids between the woven yarns of the four dir fabric. The composite is thus formed by the combination of three phases: the fibres, the Nasicon matrix (the constant $x = 1.9$ composition is checked by X-ray diffraction and Raman scattering [24]) and the interphase, with a variable composition between $ZrO_2 2SiO_2 1.5P_2O_5$ and $Na_{1.9}Zr_2Si_{1.9}P_{1.1}O_{12}$.

The boron oxide is eliminated by evaporation during the hot pressing cycle. No traces ($\leq 1\%$) can be detected by chemical or energy dispersive spectroscopy (EDX) analysis in sintered samples.

2.5. Hot pressing

Pressure sintering is performed under vacuum up to 400 °C, an N_2 atmosphere (1.01 10^5) being imposed above 400 °C. The heating rate is 250 °C h^{-1} up to

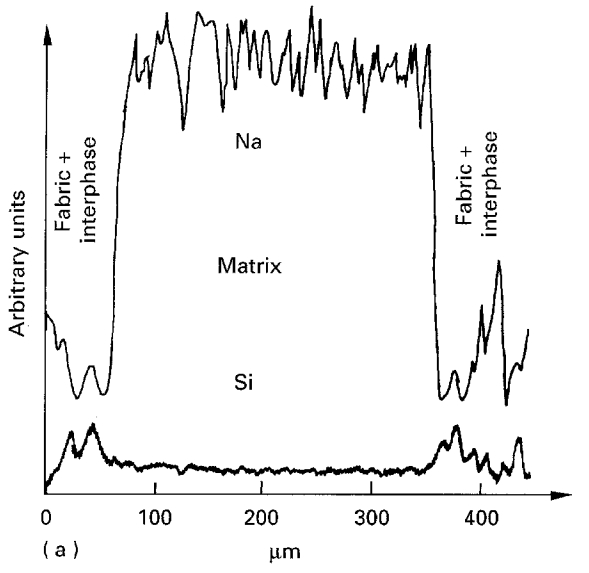

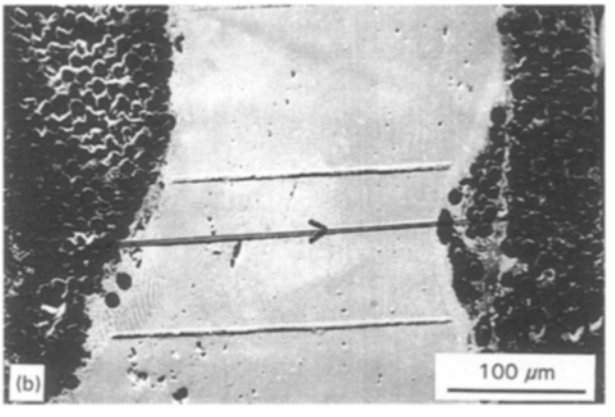

Figure 3 (a) Na and Si X-ray line scan profiles across the matrix film between two fabric reinforced regions. The average Na and Si content within the matrix are about ~13 and 10% in weight, respectively, and (b) the corresponding scanning electron photomicrograph.

600 °C and increased to 350 °C h^{-1} up to the dwell temperature. A pressure of 2.5 MPa is applied at the beginning of the hot pressing cycle in order to obtain good contact between the yarns, the interphase precursor and the matrix precursor. The applied pressure is then raised to 20 MPa between 600 and 800 °C, this final value being reached before the beginning of the start of the Nasicon shrinkage (Fig. 2). The sample dimensions are 35 × 35 × 3.5 or 50 × 50 × 3.5 mm^3. The pressure is removed just before the end of the dwell time. Cooling is complete after 5 h.

2.6. Techniques

The expansion–shrinkage measurements were achieved using an Adamel Lhormergy DI24 apparatus (Instrument SA, Longjumeau) with a silica or alumina rod and support. Curves were drawn under vacuum at heating–cooling rates of 5 °C min^{-1}.

Fracture surfaces and sliced or polished sections of the composites were observed using a 200 kV Cambridge scanning electron microscope (SEM). EDX analyses were performed using a 2000FX Jeol microscope equipped with a Tracor system (Si: Li detector) or with a Camebax microprobe.

Flexural strengths were recorded by three point bending tests using a bar specimen (35 or 50 mm length) at a crosshead speed of 0.1 mm min^{-1}. Tests were performed in air at various temperatures, after 30 min stabilization (heating rate 300 °C h^{-1}). Typically, five samples were broken for each composite at both temperatures.

Local microhardness and interfacial frictional stress, τ, were determined using a homemade Vickers microindenter instrument. Apparatus and models used for calculation are described in [25]. The load cell measures loads up to 1 N with an accuracy of about 500 μN. The capacitive displacement gauge has an accuracy of a few nanometers. The position of the indenter relative to the polished surface of the sample and the applied load were measured continuously during testing.

Tensile strengths of raw or extracted fibres (see below) were measured using a homemade apparatus. The gauge length is 10 mm.

2.6.1. Direct current (d.c.) conductivity of SiC fibres

This was measured using the four-probe method (a droplet of silver paint is added at the tip–fibre junction). A small voltage (2–4 V) was applied. The current was measured using a 416 high speed Keithley microamperemeter. Fibres were extracted from the matrix by crushing the composite and subsequently dissolving the residual matrix in HF, first at 60–80 °C and then at room temperature. After a long and careful wash in water, the fibres were dried at 100 °C over-night.

2.6.2. Microwave and radiofrequency (r.f.) conductivity

Two kinds of equipment were used at room temperature. The first method is based on measurements of the reflection and transmission moduli between 8.2 and 12.4 GHz (*X*-band), in the fundamental waveguide mode TE_{10}, using a rectangular sample (10 × 23 mm^2) set in a brass holder which fills the rectangular waveguide. After calibration with the intermediate of a short circuit and a blank holder, reflection and transmission coefficients are obtained with the help of an automated measuring system (8410B Hewlett-Packard network analyser). Both the real and imaginary parts of the permittivity and permeability are calculated. For dielectric materials ($\mu' = 1$, $\mu'' = 0$), the relative error varies between 1 (pure dielectric) and 10% (highly conducting materials). The second method uses an APC-7 coaxial line whose inner conductor is filled by the sample and loaded with characterized impedances (pure resistive or with variable phase) or a short circuit as described in [26]. The composite sample is set in the central hole of a brass disc holder. HP8510 and 4191 Hewlett-Packard systems were used to determine the complex impedance and calculate the real and imaginary parts of the permittivity by measurement of the reflection coefficient in the transmission electron microscope (TEM) propagation mode over the 1 MHz to 6–12 GHz frequency range without dismounting

the sample as described in [27]. The sample has perfect electrical contacts with outer and inner conductors of both the coaxial line and the short circuit. However, it is not possible to achieve continuous contact between the sample circumference and the holder hole. The use of a thick film of silver paint removes air capacities which can increase interfacial effects.

3. Results and discussion

3.1. Porosity and macroscopic mechanical properties

Two-dimensional fabric SiC fibre–Nasicon matrix composites prepared by the above method with pure TBB as the interface precursor exhibit room temperature fracture (Fig. 4) and a rather good linear limit of strength behaviour (~250 MPa). Low open porosities are obtained: 8 and 5% with four dir and eight-satin fabrics, respectively. The mechanical properties (Table I) are rather good: the ultimate strength corresponds to the typical values obtained for SiC–LAS composites reinforced with the same fabrics [15]. The lowering of the mechanical properties after a 2 h 750 °C anneal in air is moderate; the use of small sliced rods ($35 \times 4 \times 2\ mm^3$) enhances the corrosion rate. However, the abrupt jumps observed on the strain–stress curve, beyond the linear region indicate matrix microcracking, showing that the fibre–matrix interface is not optimized. A good interface should give rise to a gradual decrease in slope as a function of fibre breakage and pull-out.

The use of an advanced interface precursor, a mixture of TBB, TBP, ZrP and TEOS (called Zr–Si–P–B interface precursor: volume ratios have been given

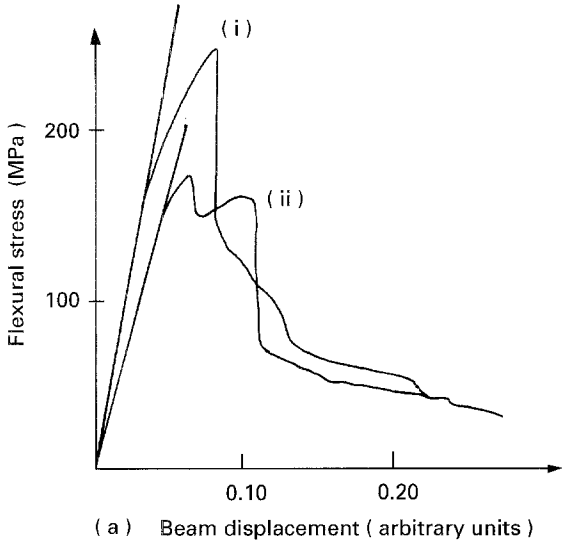

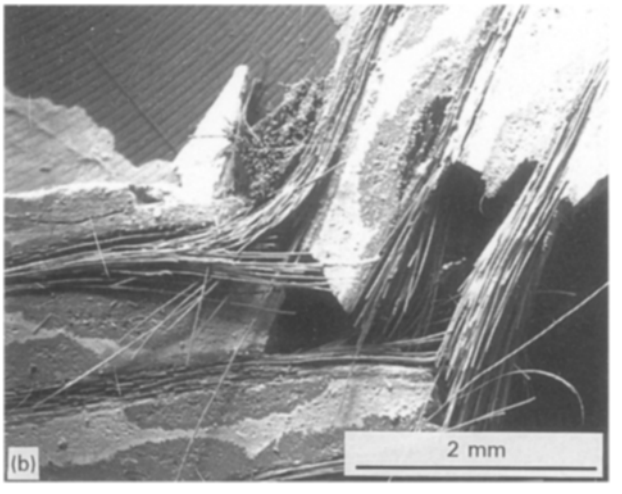

Figure 4 (a) Stress-strain plots recorded at room temperature for a SiC fibre (eight-satin) reinforced Nasicon matrix composite prepared using TBB as interface precursor: (i) after manufacturing, and (ii) after 2 h treatment in air at 750 °C, (b) an example of the fibrous fracture.

TABLE I: Structural and mechanical characterization of SiC Nicalon® NLM 202 fibre reinforced Nasicon matrix composites

Fabric	Interface precursor IP (vol ratio)	Matrix precursor MP	Hot pressing temperature, (°C) dwell time (min)	τ_F vol. (%)	ρ (g cm^{-3})	open porosity Πo (%)	Matrix	Mechanical properties σ^e_{max} (MPa)	ε^f_{max} (%)
Four dir SiC, four sheets Eight-satin SiC four sheets	2 TBB[a] + 1 acetone	Nasicon[b] ($x = 1.9$) powder gel heated for 10 h at 750 °C in air	1035, 30	42	2.70	5.0	Nasicon R[c] + ZrO_2 (t)[d]	80	0.13
			1035, 12	50	2.75	8.0	Nasicon R + ZrO_2 (m + t)	100	0.16
			1035, 45	51	2.60	6.5	Nasicon R + ZrO_2 (m)	250	0.57
Four dir SiC, four sheets	1 PZr + 1 TEOS + 1.8 TBP + 1.8 TBB		1035, 45	33	2.75	8.0	Nasicon R + ZrO_2 (m + t)	180	0.45
			1100, 10	36	2.85	9.0	Nasicon M + ZrO_2 (m)	220	0.45
Four dir SiC, two sheets + satin mullite four sheets			1070, 20	30 + 10	2.96	8.0		100	-

[a]Alkoxides: TBB, $B(OC_4H_9)_3$; PZr, $Zr(O_nC_3H_7)_4$; TEOS, $Si(OC_2H_5)_4$; TBP: $PO(O_tC_4H_9)_3$
[b]Nasicon ($x = 1.9$): $Na_{2.9}Si_{1.9}P_{1.1}Zr_2O_{12}$.
[c]R, rhombohedral ($R\bar{3}c$) Nasicon; M, monoclinic ($C2_c$) Nasicon
[d]m, monoclinic; t, tetragonal.
[e]Ultimate flexural strength.
[f]The strain is calculated from the bending displacement according the following formula, $\varepsilon = 6h\delta F/D^2$, where F is the applied load, D the distance between knives, and h is the thickness of the sample.

earlier) leads to a precursor which exhibits a higher viscosity and ceramic yield. Optimization of the sintering is possible. Fig. 5 compares the evolution of open porosity (measured by comparison of the dry mass, the Archimedean mass and the wet mass of the composite) and the flexural strength as a function of the applied pressure during the dwell time. It is clear that the applied pressure enhances the densification. The threshold required to reach a low porosity is 15 MPa. Optimization of the dwell temperature can be achieved according to both microstructural and crystallographic criteria. However, previous studies have shown that sol–gel prepared Nasicon must be heated to over 950 °C for it to crystallize into the rhombohedral ($R\bar{3}c$) phase, and to over 1100 °C for it to transform at room temperature to the monoclinic C2/c) phase [23]. This structural change is related to the level of orientational disorder of SiO_4 and PO_4 tetrahedra imposed by the heating temperature; this level determines the activation energy and the value of electrical conductivity, especially in the microwave range [23, 27].

On the other hand, degradation of the Nicalon® NLM202 fibres takes place above 1350 °C in vacuum [28] but at lower temperatures in the presence of alkali or earth alkali ions [29, 30]. Furthermore, Nasicon $x = 1.9$ solid solution melts incongruently at about 1275 °C [8]. The range of temperature in which the sintering of the composite may occur is thus between 950 and 1200 °C.

The optimization of porosity and mechanical properties was achieved at temperatures between 1035 and

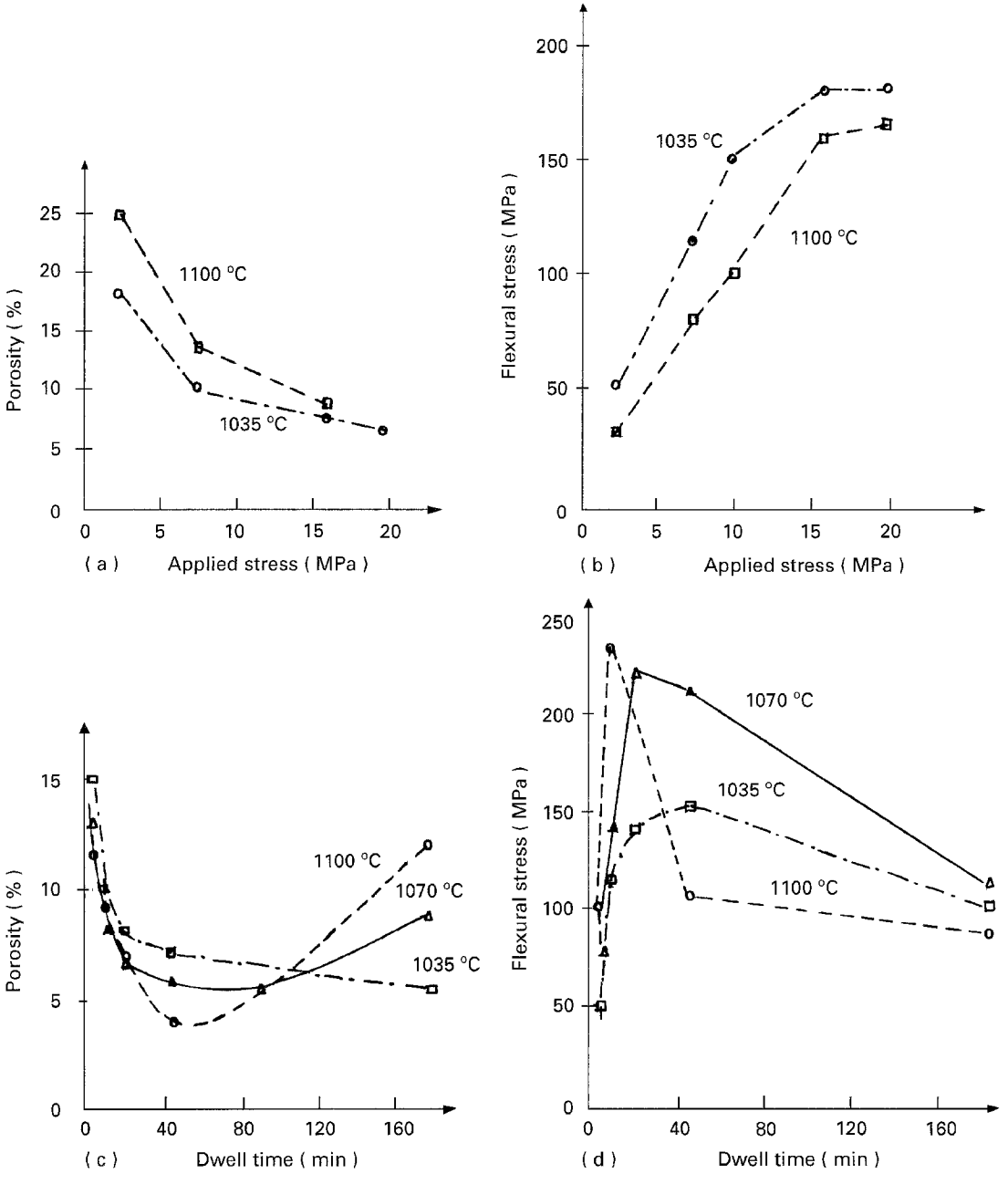

Figure 5 Plots of the open porosity (a) and of the room temperature three point bending strength of SiC Nasicon composites (b) as a function of the pressure applied during hot pressing for dwell conditions: (-·-·-) dwell temperature, 1035 °C; dwell time, 45 min. (- - -); dwell temperature, 1100 °C; dwell time, 10 min. Four dir fabric and Zr–Si–P–B interface precursor are used. Plots of the open porosity (c) and of the ultimate flexural stress (d) are given versus dwell times for a 20 MPa hot pressing at 1035, 1070 and 1100 °C (four dir fabric and Zr–Si–P–B interface precursor are used).

1100 °C using the four dir fabric. The lowest porosity and highest mechanical strength were achieved for different temperature–dwell time couples (Fig. 5c, d). However, the high temperature enhances the kinetics of the fibre–sodium and phosphorus ion reactions [29, 30]. An increase in the porosity is observed for long dwell times in correlation with degradation of the fibre [24]. The temperature range in which SiC fibre reinforced Nasicon composites can be prepared is thus 1035–1070 °C. In this range, the mechanical properties are not very sensitive to the dwell-time, enabling reproducible manufacture. The mechanical properties are stable up to 600 °C in air. Fig. 6 gives an illustration of the stress–strain plots obtained using the optimized process. The smooth and regular decrease after the ultimate strength value indicates that considerable fibre pull-out occurs.

3.2. Stress–stain curves and interphase/interface behaviour

Monolithic Nasicon ceramics exhibit low mechanical properties (about 100 MPa). This low value has been attributed to a microcracking phenomenon associated with the monoclinic–rhombohedral phase transition at 160 °C [12, 31]. The presence of microcracks in the Nasicon matrix can explain the rapid departure from linear behaviour observed on stress–strain plots whatever the fabric used (Figs 4 and 6). Departure from the elastic behaviour is observed at about 40% of the break value, whereas the elastic limit is usually 0.6–0.7 times the ultimate strength in composites using a high strength matrix, e.g. mullite as matrix [16]. The thermal expansivities $\alpha_{25-600\,°C}$, measured along the woven fabric sheet (//) and perpendicularly ($\perp$) are 3.9 and $5.3 \times 10^{-6}\,°C^{-1}$, respectively. The corresponding value for pure Nasicon solid solution is $5.5\ 10^{-6}\,°C$ [8]. The fibre network forces the matrix to expand, which unfortunately leads to microcracking. Composites reinforced simultaneously with SiC Nicalon and mullite Nextel fibres are prepared by the same method. However, due to the lower tensile strength of Nextel fibres (about 1300 MPa for a 1100 °C thermal treatment [19]), the resulting strengths of mixed SiC–mullite fibre reinforced Nasicon matrix composite are lowered (Table I).

In the four dir fabric, the fibres are woven along four directions in the plane (0^d, 45^d, 90^d, 135^d, see Fig. 1). This implies that only 25% of the fibres "work" during the bending test. By taking into account the fibrue volume (~ 0.4, Table I), one can assume that the ultimate strength of the composite is given by the following formula:

$\sigma_c = 0.25 \times$ fibre volume $\times$ tensile strength value of the fibres (σ_f)

The last parameter has been measured on extracted fibres. Two distributions of fibres were observed. The average values were about 2200 and 1200 MPa, respectively (see below). The results given in Table I are consistent with this phenomenological law ($\sigma_c \sim 0.1\sigma_f$). Using satin fabric, the proportion of fibres stressed in a bending test is increased by a factor two. Thus, the expected value may reach, e.g., $\sim$400 MPa when

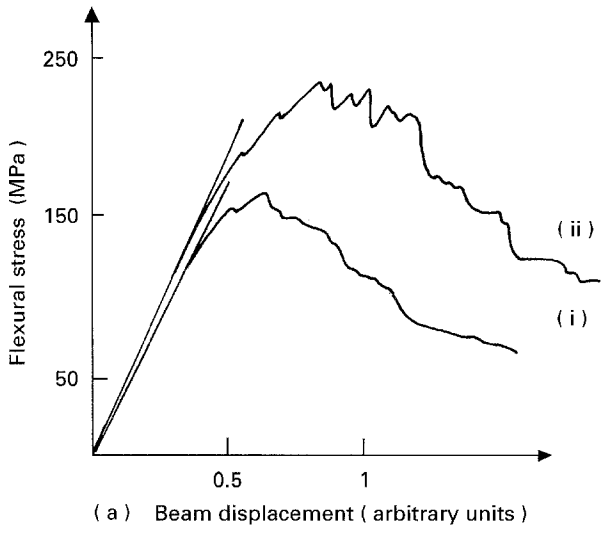

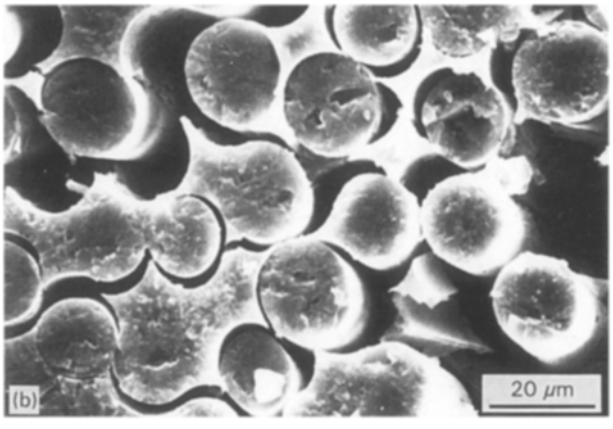

Figure 6 Stress-strain plots recorded at room temperature (i) and at 400 °C in air (ii) for a composite hot pressed at 1035 °C for 45 min using Zr–Si–P–B interface precursor and four dir fabric. (b) Good fibre–interphase debonding is shown on a sample which is broken before polishing.

$\sim$200 MPa is obtained using four dir fabric. However, the preparation of "good" satin reinforced composites is hindered by the high density of yarn packing which requires a low viscosity sintering aid, leading to increased fibre corrosion (see below).

Fig. 7 shows SEM photomicrographs and the corresponding X-ray line scan profiles recorded with a Camebax electron microprobe across the SiC fibres. Na, Si, C and P profiles are measured. The fibrous fracture observed in silicate matrix composites is usually explained by the presence of a graphitic carbon film at the SiC fibre–matrix interface [32–35]. Microanalysis shows that Na diffusion occurs within the fibre core in Nasicon matrix composites even with the interposition of an Na-free interface precursor between the fibre and the Nasicon matrix as a diffusion barrier (Fig. 3). Chemical analysis of extracted fibres and *in situ* EDX analysis give the same: Na/Si atomic ratio ($\sim$2%). Furthermore, as shown in Fig. 7, one observes a black contour around the fibre using the backscattered electron mode. Microanalysis shows that P replaces Si and that the Na content also increases at the periphery of the fibre. The oxygen content is increased to satisfy the electrical balance, but a carbon rich contour is observed at the boundary between the fibre core and the dark crust. A reasonable assumption is that the oxycarbide second phase

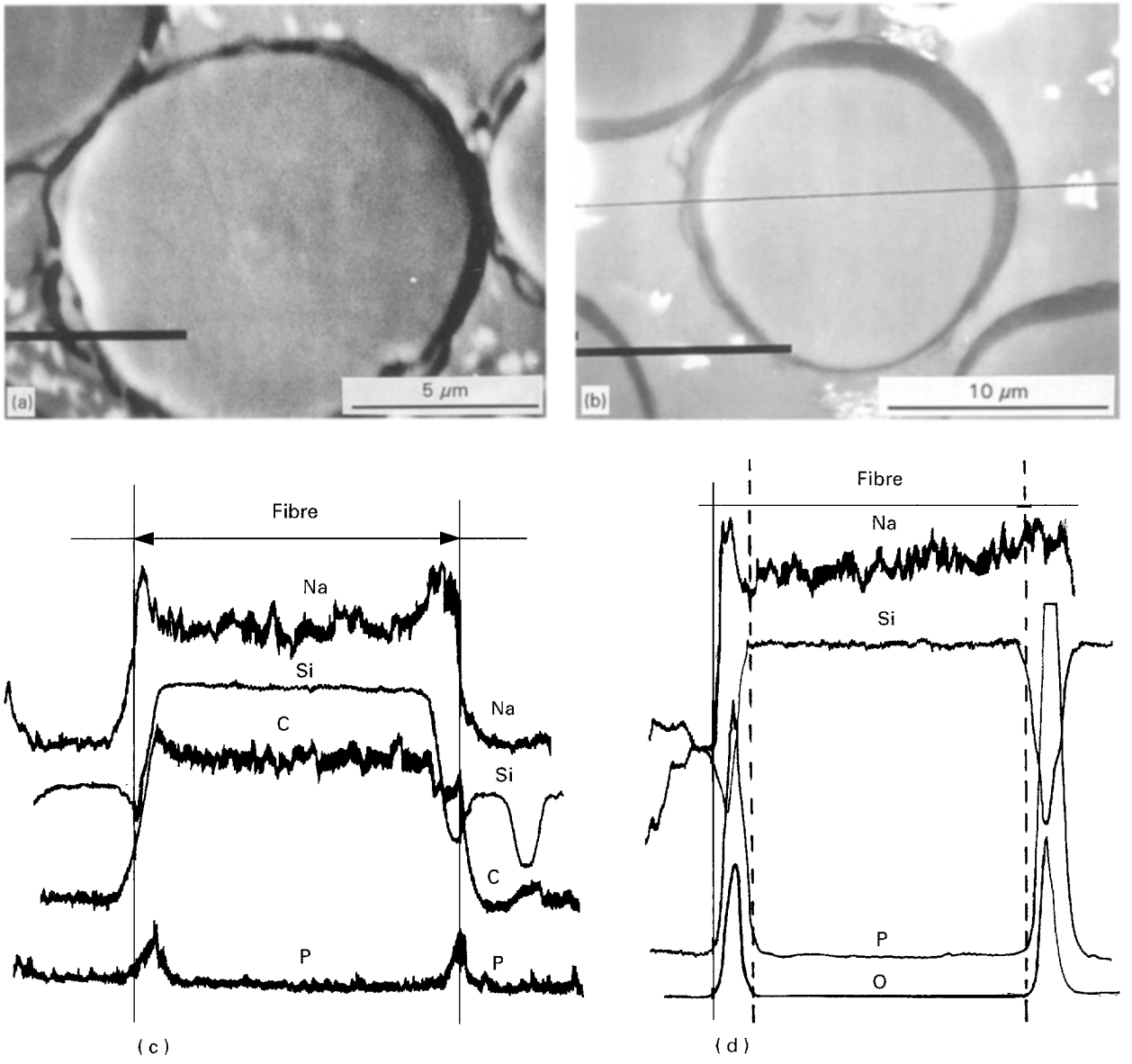

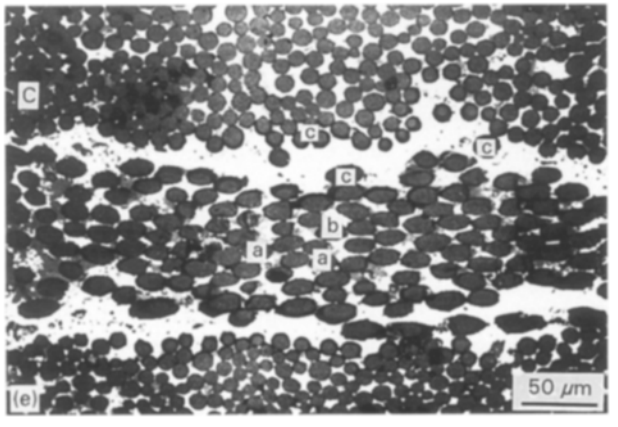

Figure 7 SEM photomicrographs (a, b) and X-ray line scan profiles (c, d) recorded across SiC Nicalon® NLM 202 fibre sections embedded in pyrolysed Zr–Si–P–B interface precursor. Na, Si, C, P and O profiles are measured for a fibre exhibiting a small ("a" fibre type) and a medium ("b" fibre type) reaction crust. Examination of the photomicrograph given in (e) shows that "c" fibres are located at the external surface of the fabric sheets where the concentration of Na ions is increased.

of SiC Nicalon® NLM202 fibre undergoes the following reaction

$$SiO_{4-x} + C_x + yNa^+ + zP^{5+} \rightarrow Na_y(Si_{1-z})O_{4-x+\frac{y}{2}+\frac{5}{2}z} + xC$$

3.3. Relationship between interfacial reaction and mechanical properties

The high strength and toughness of ceramic matrix composites result directly from the "low" fibre–matrix bonding produced by the processing. Usually, reaction between the SiC Nicalon fibres and the melted glass–ceramic matrix leads to the formation of a "thin carbon-rich interfacial layer" (~ 100 nm), referred to as the carbon interphase [32–34, 36]. As pointed out above, this interphase acts as a "fuse" deflecting the matrix microcracks parallel to the fibre axis and thus avoiding early failure of the fibres. This sliding interphase is formed *in situ* during injection of the melted matrix within the fibre preform as a result of the fibre–matrix reaction (alkali or earth alkali containing silicate matrix) or results from the deposit of a thin coating of C or BN [35] or of ZrO_2 [19] when non-reactive matrices are used. In the first case, underline that the reaction is strong (molten salt with a high concentration of alkali ions) but short (a few minutes, usually), whereas the reaction time is longer in the present process.

Micro-Vickers indentation shows that the crust is a glass (Vickers hardness, $H_V \sim 5$–6 GPa) [25, 37, 38], whereas the SiC fibre core retains the mechanical properties ($H_V \sim 25$ GPa) of an unreacted fibre. Thus, in a composite, the fibres can be classified into three types:

1. "a" fibres exhibiting no visible crust at this examination scale (resolution ~ 0.1 μm), these "a" fibres are located in the fabric inner region,
2. "b" fibres exhibiting a visible but small contour (~ 1.5 μm), these fibres are located at the fabric surface, and
3. "c" fibres exhibiting a large crust, such as shown in Fig. 8. Measurements of the tensile strength of extracted fibres show that the "a" and "b" fibres retain roughly the same tensile strength (2100–2400 MPa; gauge length, 10 mm). This value is similar to that observed for fibres heated to the same temperature in an N_2 atmosphere. On the other hand, the "c" fibres have a tensile strength between 1100 and 1300 MPa. In fact, the tensile stress value is lower, a large number of fibres being broken during handling. The required mechanical strength for a fibre to be handled safely is about 1000 MPa.

Determination of the relative proportion of "a", "b" and "c" fibres on polished sections of composites by visual selection shows that optimized mechanical properties are observed for composites containing 10, 60 and 30% of "a", "b" and "c" fibres, respectively. Microindentation confirms that the formation of a "large" reaction zone at the fibre contour lowers both the interfacial shear stress, τ, and the sliding load threshold [37, 38]. Chemical attack on the SiC Nicalon® fibre appears necessary to obtain good mechanical properties. Indentation plots and SEM examination show that interfacial sliding occurs both at the fibre–crust and crust–matrix interface.

The sliding strength was measured as described in [25], following a method related to the Marshall method previously established for one-dimensional composites [36]. The position of the indenter relative to the polished surface of the sample and the applied load were measured continuously during testing [25]. Two regions are clearly distinguished on the load, F,–depth, h, plots (Fig. 8a)

1. First, a polynomial regime, $h = \alpha F^{\beta}$ (Meyer law), related to the fibre indentation and its elastoplastic deformation under the sharp indenter [25, 39].
2. A region characterized by a lower rate of load increase, a few steps often being observed at the limit between the elasto–plastic response of the fibre and the debonding-plus-sliding regime (in relation to the two debonding interfaces, interphase–crust and crust–core). The fibre curvature in four direction woven fabric is sufficiently large (radius > a few centimeters) and the debonding length (50–500 μm) sufficiently small to make experiments and calculations possible. Comparison with experiments (using the same model and instrument) on SiC–LAS matrix composites (threshold load for debonding, Fs, ~ 10–15 g; frictional shear stress, τ, ~ 3–8 MPa) shows that the interfacial shear stress is lowered in fibres exhibiting a reaction crust ("a" fibre, $\tau > 50$ Mpa; "b" fibre, $\tau = 38 \pm 8$ MPa; "c" fibre, $\tau = 27 \pm 8$ MPa; the threshold load, $Fs \sim 20$–25 g, appears similar for "b" and "c" fibres.

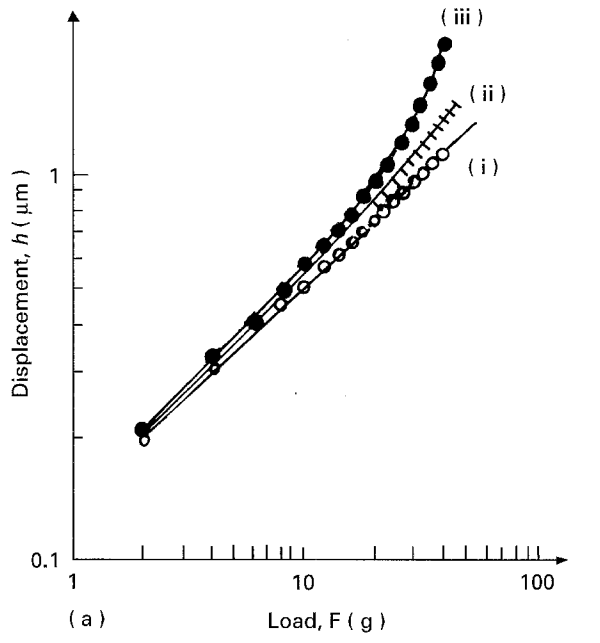

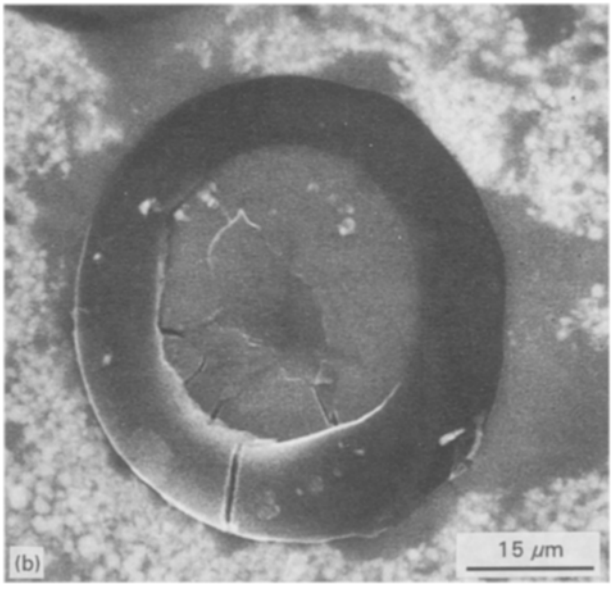

Figure 8 (a) Typical experimental depth–load traces for microindented Si–C Nicalon® NLM202 fibre are shown using a log–log plot for the three types of fibres: (i) unreacted "a" fibre, no sliding; (ii) "b" fibre exhibiting a medium reaction crust; (iii) "c" fibre exhibiting a large crust. In these last two cases departure from the linear behaviour (elasto–plastic response of the fibre according Meyer's law, $h = \alpha F^{\beta}$) makes the sliding visible. (b) SEM of microindented SiC–Nicalon® NLM202 fibre with a large reacted crust ("c" fibre type). Double debonding step, and crust microcracking are visible at the matrix–crust and crust–core fibre interface. The white dots correspond to zirconia precipitates in the interphase originating from the pyrolysis of the Zr–Si–P–B interface precursor.

4. Electrical properties

Electrical properties can be determined at various frequencies [40–44]. The interaction between electromagnetic waves and condensed matter can be described using complex permittivity, ε^*, and conductivity, σ^*, concepts. The relation between the real part of

the (polarization) conductivity, $\sigma'(\omega)$, and the imaginary part of the permittivity, $\varepsilon''(\omega)$, is $\sigma'(\omega) = \omega\varepsilon''(\omega)$, ω being the angular frequency. In the high frequency region, i.e. the infrared region, there are various resonances arising from ionic, molecular and (at higher energy) electronic motion. At lower frequency, i.e. in the microwave and radiofrequency range, dipolar and space charge relaxations are observed. The low frequency domain corresponds to "free charges" which can move in response to the electric field (a diffusion current results from the field propagation), while the region at high frequencies is dominated by "bound charges" (dipoles) corresponding to the oscillating character of the electromagnetic wave (polarization current) [43–45]. Overlap with relaxation is often observed [45].

Using crude models with non-interacting or "free" charges, a constant value of conductivity versus frequency is expected. The constant conductivity is related to the fact that a randomly hopping charge has no memory, hence any hop should be correlated to itself. On the other hand, trapped charges lead to the formation of frequency dependent conductivity. Considering an approach based on the concept of "localized states" in semiconducting materials, Mott and Davis [40–42], developed microscopic models to describe the $\sigma'(\omega) = A\omega^s$ experimental law (A^2 constant). Similar approaches has been used for ionic conductors in which the transport of the mobile ions is strongly influenced by their mutual repulsive interactions, and so their hopping motion is not expected to be a purely random process [45–48]. Unsuccessful hops cause a dispersive conductivity, i.e. a transition from a constant low frequency conductivity to a power law behaviour ($\sigma = \sigma_{d.c.} + A\omega^s$). The parameter s is related to the β parameter of the Debye relaxation of "localized charges" [44–46] ($D = 1 - \beta$, $s \lesssim 1$)

$$\frac{\varepsilon(\omega) - \varepsilon(\infty)}{\varepsilon(0) - \varepsilon(\infty)} = \left(\frac{1}{1 + j\omega\tau}\right)^{\beta}$$

where ε_∞ and ε_0 are limiting values of $\varepsilon^*(\omega)$ as ω goes to the optical, ε_∞, and static, ε_0, limits, τ being the Debye relaxation time [44, 45].

4.1. D.c. Conductivity

Fig. 9 compares the room temperature d.c. conductivity of fibres extracted from composites with that of fibres heated in N_2 to low (500 °C) and high (1200 °C) temperatures. A temperature of 1200 °C can be considered as the starting point of carbon precipitation at the fibre surface in N_2 atmosphere [2], whereas 500 °C is considered as the temperature which cleans the weaving aids from the surface. The results confirm the previous work of Chauvet *et al.* [2]. Fibres extracted from a composite hot pressed at 900 °C show the same conductivity as the 1200 °C N_2 heated fibres. One emphasizes that no fibre reaction is observed in such composites by SEM or X-ray microprobe analysis. On the other hand, fibres extracted from 1035 °C hot pressed composites, i.e. from composites with optimized mechanical properties in which a large number of fibres exhibit a reaction crust, have a very high conductivity ($\sim 10\ S\ m^{-1}$).

4.2. Radio frequency and microwave conductivity

The high frequency conductivity of composites No. 1 and 2 is larger than that of the Nasicon matrix and of the fibre heated to 1200 °C in an N_2 atmosphere, although the composites are porous, which lowers slightly the apparent conductivity. The main difference between the two composites is their fibre volume content (composite No. 1, 44%; composite No. 2, 33%). The higher conductivity of composite No. 1 can thus be assigned to the higher proportion of fibres, the reacted fibres having a conductivity at least two orders of magnitude shown higher than that of the Nasicon matrix. The conductivity of SiC Nicalon fibres heated to 1200 °C in N_2 is shown in Fig. 9. Drude behaviour is observed up to ~ 1 GHz. Above this a relaxation contribution is observed which is assigned to the presence of nanometric carbon precipitates in the Nicalon fibre [2]. The conductivity of the composites exhibits a similar Drude behaviour (no frequency dependence) in the whole range studied. On the other hand, the conductivity of the air treated composite (Table II) shows a frequency dependent conductivity very similar to that observed in poorly conducting Nasicon [27]. It can thus be concluded that the high conductivity of the composite is mainly due to the carbon rich fibre "crust" resulting from the degradation of the SiC Nicalon fibre. The fact that d.c. conductivity exhibits a similar value indicates that carbon precipitates form a percolating network. The disappearance of Drude behaviour after heating in air is consistent with the carbon burning. Examination of the fibre after an 800 °C air treatment shows a destruction of the fibre crust [24].

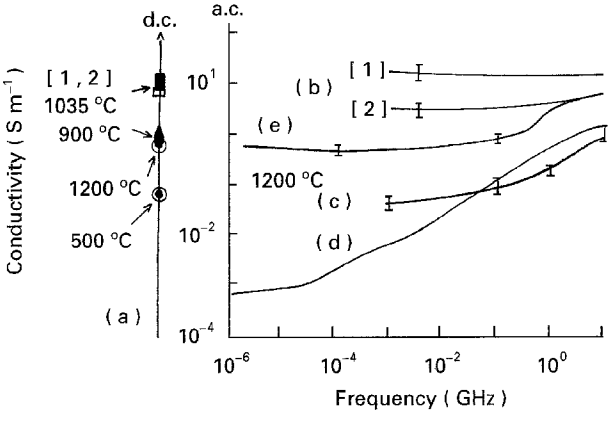

Figure 9 Comparison between the room temperature d.c. conductivity (a) of SiC Nicalon® NLM202 fibre heated at 500 and 1200 °C under N_2 (circles) and of fibres extracted from composites hot pressed at 900 and 1035 °C: ((■) composite No. 1: open porosity: 8%; fibre volume, 0.44. (□) Composite No. 2: open porosity, 14%; fibre volume, 0.33). And (b) of the radio frequency to microwave conductivity of composites Nos 1 and 2. The conductivity of pure Nasicon matrix and of a composite heated a few hours in air at 750 °C is given in (c) and (d), respectively. Curve (e) corresponds to the conductivity of SiC Nicalon® NLM202 fibre heated for 2 h at 1200 °C under N_2 (after [2]) (typical error bars are given).

Plots of ε' versus frequency are given in Fig. 10. The curves of pure $x = 1.9$ Nasicon ceramic are very similar to that of the 750 °C air annealed No. 3 composite. However, real permittivity is not greatly affected by the presence of a procolating second phase: the permittivity of a phase mixture can be described using a phenomenological law, e.g. the Looyenga model or Wagner model [49], in which the average permittivity is a polynomial function of the phase concentration. Furthermore, the real permittivities of SiC and Nasicon are not very different, $\varepsilon'^{SiC}_{10\ GHz} \approx 20$[2] and $\varepsilon'^{Nasicon}_{10\ GHz} = 16$, respectively, [27]. The plots of ε' versus frequency clear kinks which indicates that dipolar relaxations are present. The plot of imaginary permittivity, ε'', versus real permittivity (Cole–Cole plot) for the annealed composite No. 3 is composed of two semicircles, after subtraction of the low frequency part originating from the electrode–ceramic interface as described in [27]. These relaxations are centred at 28 and 575 MHz, corresponding to relaxation times

TABLE II Electrical properties of SiC (mullite) fibre–Nasicon matrix composites and constituents

Material	Hot pressing temperature (°C) dwell time (min)	Open porosity, π_o (%)	τ_F vol (%)	10 GHz properties					
				X band		APC7		σ	s^a
				ε'	ε''	ε'	ε''	(S/m)	
Matrix									
Mullite	1350, 30	1.0	–	5.0	–	–	–	–	–
Nasicon matrix ($x = 1.9$)	1000, 30	0.5	–	15.3	4.0	–	–	–	–
	1100, 30	0.5	–	16.6	5.2	–	–	–	–
Composite									
Four dir, No. 1 four sheets	1035, 45	8.0	44	40.0	50.0	50	30	18	~ 0.90
No. 2	1035, 45	14.0	33	16.0	50.0	16	15	8	~ 0.85
No. 3	1035, 45 + 750, 120 air	6.5	46	–	–	10	4	2	~ 0.85
Four dir, two sheets + Nextel satin, four sheets	1070, 20 + 600, 120 air	8.0	30 10	30.0 10.0	40.0 15.0	–	–	–	–

[a]Exponent of the ω^s law.

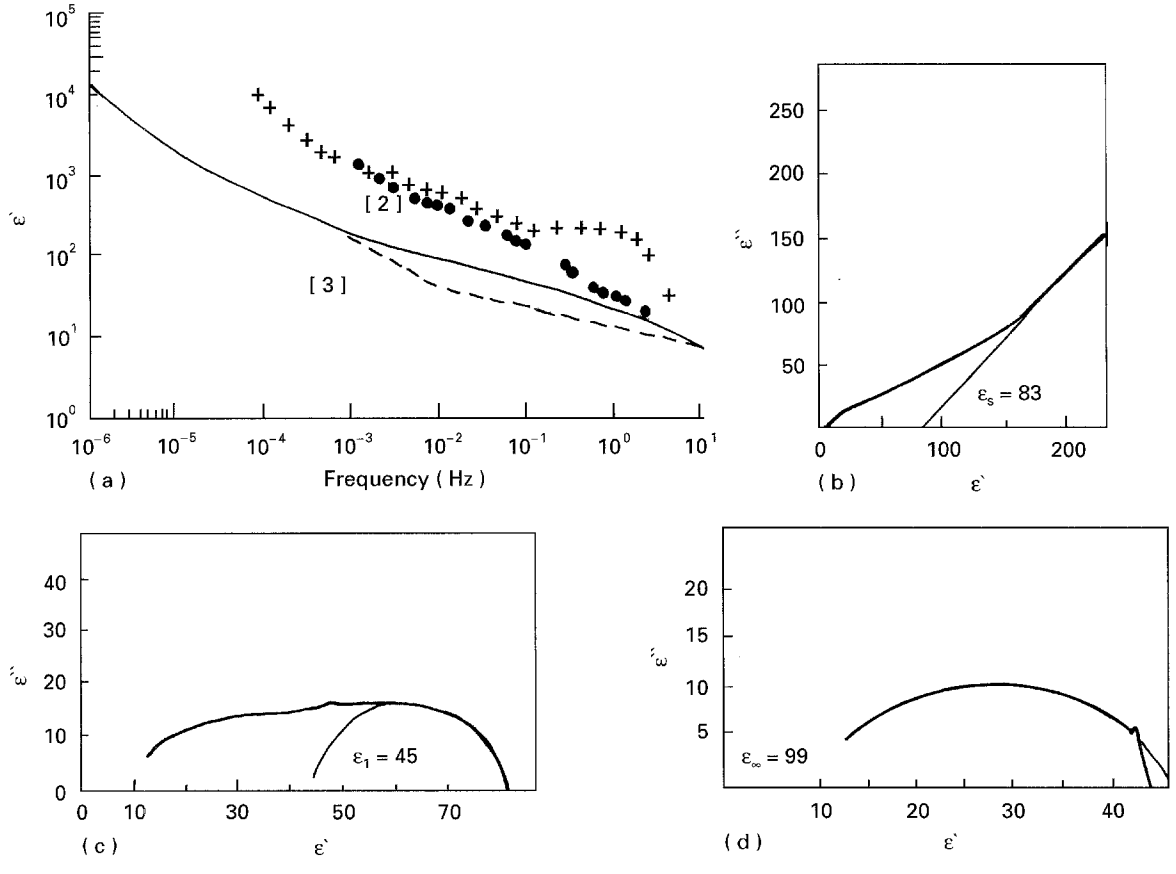

Figure 10 Comparison of ε' versus frequency for (a) pure Nasicon ceramic (- -), SiC fibre heated at 1200 °C under N_2 (+) (after [2]), of composite No. 2 and of 750 °C air annealed composite No. 3. The corresponding Cole–Cole plot $\varepsilon'' = f(\varepsilon')$, of this last sample is given in (b); details: (c) plot exhibiting the two relaxations (the low frequency straight line has been subtracted according to the method described in [26]); (d) plot showing the high frequency relaxation, the low frequency relaxation being subtracted.

of 3.55×10^{-8} s and 1.75×10^{-9} s, respectively. The semicircles are off-centred, which indicates a deviation from the Debye model caused by interaction between dipoles. This 10^{-8} s relaxation has already been observed in pure Nasicon ceramics and assigned to ferroelectric local ordering, which disappears at monoclinic–rhombohedral phase transitions at about 160 °C [27, 6]. The second relaxation (1.7×10^{-9} s) occurs in the same domain as the relaxation observed for the 1200 °C annealed SiC fibre [2], and can be thus assigned to the fibre (with its crust).

5. Conclusions

Almost fully dense Nasicon matrix composites have been prepared by a sol–gel route using a tailored interface precursor compatible with SiC Nicalon or mullite Nextel fibres. Good mechanical properties are obtained for SiC–Nasicon composites (~250 MPa) up to 600 °C.

The "sliding" carbon-rich interphase formed by reaction of SiC Nicalon® NLM202 fibres with an alkali-rich matrix is more complex than a simple C film. The origin of carbon precipitation is found to be the attack of the oxycarbide second phase by Na and P. A sliding interface occurs both at the matrix–reacted fibre and at the reacted fibre–unreacted fibre core boundary. The conducting properties of untreated SiC–Nasicon composites are dominated by the electrical properties of the reacted fibre crust containing C precipitates (and thus not stable above 700 °C in air). The electrical properties of the composite are functions of the relative volume of matrix and (reacted) fibres and of the fibre nature (Table II).

References

1. A. G. EVANS, *J. Amer. Ceram. Soc.* **73** (1990) 187.
2. O. CHAUVET, T. STOTO and L. ZUPPIROLI, *Phys. Rev. B* **46** (1992) 8139.
3. H. G. SOWMAN and D. D. JOHNSON, in "Fibre Reinforced Ceramic Composites", edited by K. S. Mazdiyasni (Noyes, Park Ridge, NJ, 1990) pp. 127–138.
4. G. PARTRIGE, *Angew. Chem. Int. Eng., Adv. Mater.* **328** (1989) 1746.
5. K. M. PREWO and J. J. BRENNAN, *J. Mater. Sci.* **17** (1982) 2371.
6. J. P. BOILOT, Ph. COLOMBAN and G. COLLIN, *Solid State Ionics* **28/30** (1988) 403.
7. R. ROY, J. ALAMO, D. K. AGRAWAL and R. A. ROY, *Mater. Res. Bull.* **19** (1984) 471.
8. Ph. COLOMBAN and E. MOUCHON, *Solid State Ionics* **73** (1994) 209.
9. K. S. MAZDIYASNI, *Ceram. Int.* **8** (1982) 42.
10. D. W. JOHNSON Jr, *Amer. Ceram. Bull.* **64** (1985) 956.
11. L. C. KLEIN (editor), "Sol–Gel Technology" (Noyes, Park Ridge, NJ, 1988).
12. Ph. COLOMBAN, *Ceramic Int.* **15** (1989) 23.
13. V. VENDANGE and P. COLOMBAN, *J. Sol-gel Sci. Technol.* **2** (1994) 407.
14. Ph. COLOMBAN and V. VENDANGE *J. Non-crystalline Solids* 1478. **148** (1992) 245.
15. Ph. COLOMBAN, M. MENET, E. MOUCHON, C. COURTEMANCHE and M. PARLIER, French Patent FR2 672 283, August (1992), European Patent 92 400 235.5, US Patent 7/930 804.
16. Ph. COLOMBAN and E. MOUCHON, in "High-temperature Ceramic Matrix Composites", Proceedings HT-CMC1, Bordeaux, September 1993, edited by R. Naslain, J. Lamon and D. Doumeingts (Woodhead, Abington, 1993) pp. 159–166.
17. P. COLOMBAN, in Proceedings JNC-8 (8ème Journées nationales sur les composites), Palaiseau, November 1992, edited by O. Allix, J. P. Favre and P. Ladevèze (AMAC, Paris, 1992) pp. 73–84.
18. E. BRUNETON, D. MICHEL, J. L. PASTOL and P. COLOMBAN, in *ibid.* pp. 253–264.
19. E. MOUCHON and Ph. COLOMBAN, *Composites* **26** (1995).
20. Ph. COLOMBAN, E. BRUNETON, J. L. LAGRANGE and E. MOUCHON, *J. Eur. Ceram. Soc.* (1996) in press.
21. H. PERTHUIS and Ph. COLOMBAN, *Ceramic Int.* **12** (1986) 39.
22. Ph. COLOMBAN, *Adv. Ceram.* **21** (1987) 139.
23. *Idem, Solid State Ionics* **21** (1986) 97.
24. E. MOUCHON, PhD thesis, University of Paris VI (1992).
25. J. L. LAGRANGE, B. PASSILLY, M. PARLIER and P. COLOMBAN, in Proceedings JNC-8 (8ème Journees nationales sur les composites), Palaiseau, November 1992, edited by O. Allix, J. P. Favre and P. Ladevèze (AMAC, Paris, 1992) pp. 241–252.
26. N. BELHADJ-TAHAR and A. FOURIER-LAMER, *L'Onde Electrique* **68** (1988) 50.
27. Ph. COLOMBAN, E. MOUCHON, N. BELHADJ-TAHAR and J. C. BADOT, *Solid State Ionics* **53–56** (1992) 813.
28. J. LIPOWITZ, *Amer. Ceram. Soc. Ceram. Bull.* **70** (1991) 1888.
29. E. MOUCHON. and Ph. COLOMBAN, *J. de Physique IV* **C7** (1993) 1941.
30. Ph. COLOMBAN, in Proceedings of Ceramic–Ceramic Composites III, October 1994, Mons, (silicates Industriels).
31. I. YAMAI and T. OTA, *J. Amer. Ceram. Soc.* **76** (1993) 487.
32. R. F. COOPER and K. CHYUNG, *J. Mater. Sci.* **22** (1987) 3148.
33. L. A. BONNEY and R. F. COOPER, *J. Amer. Ceram. Soc.* **73** (1990) 2916.
34. J. J. BRENNAN, in "High-temperature Ceramic Matrix Composites", Proceedings HT-CMC1, Bordeaux, September 1993, edited by R. Naslain, J. Lamon and D. Doumeingts (Woodhead, Abington, 1993) pp. 269–283.
35. R. NASLAIN, in Proceedings JNC-8 (8ème Journées nationales sur les composites), Palaiseau, November 1992, edited by O. Allix, J. P. Favre and P. Ladevèze (AMAC, Paris, 1992) pp. 199–212.
36. D. B. MARSHALL, *J. Amer. Ceram. Soc.* **67** (1984) 259.
37. E. MOUCHON, J. L. LAGRANGE and Ph. COLOMBAN, in Proceedings JNC-8 (8ème Journées nationales sur les composites), Palaiseau, November 1992, edited by O. Allix, J. P. Favre and P. Ladevèze (AMAC, Paris, 1992) pp. 85–96.
38. S. BLEAY, V. D. SCOTT, B. HARRIS, R. G. COOKE and F. A. HABIB, *J. Mater. Sci.* **27** (1992) 2811.
39. J. L. LOUBET, J. M. GEORGES and G. MEILLE, in "Microindentation techniques in Material Science and Engineering", edited by P. J. Blau and B. R. Lawn (American Society for Testing Materials, STP 889, Philadelphia, PA, 1986) pp. 72–89.
40. N. F. MOTT and E. A. DAVIS, "Electronic Processes in Non-crystalline Materials" (Clarendon, Oxford, 1979).
41. S. R. ELLIOT and A. P. OWENS, *Phil. Mag. B* **80** (1989) 777.
42. H. KAHNT, *Ber. Bunsenges Phys. Chem.* **95** (1991) 1021.
43. A. K. JONSCHER, "Dielectric Relaxation in Solids" (Chelsea Dielectric Press, London, 1983).
44. P. DEBYE, "Polar Molecules" (Dover, NY, 1945).
45. Ph. COLOMBAN and J. C. BADOT, *Solid State Ionics* **61** (1993) 55.
46. K. FUNKE, *Ber. Bunsenges Phys. Chem.* (1991) 955.
47. A. A. VOLKOV, G. V. KOZLOV and J. PETZELT, *Ferroelectrics* **95** (1989) 23.
48. M. D. INGRAM, P. MAASS and A. BUNDE, *Ber. Bunsenges Phys. Chem.* **95** (991) 1002.
49. J. B. BIRKS, "Progress in Dielectrics", Vol. 7 (Heywood Books, London, 1967) pp. 71–113.

Received 27 January
and accepted 11 May 1995